



1 A Two-Component Parameterization of Marine Ice Nucleating 2 Particles Based on Seawater Biology and Sea Spray Aerosol 3 Measurements in the Mediterranean Sea

4 Jonathan V. Trueblood¹, Alesia Nicosia¹, Anja Engel², Birthe Zäncker², Matteo Rinaldi³, Evelyn
5 Freney¹, Melilotus Thyssen⁴, Ingrid Obernosterer⁵, Julie Dinasquet^{5,6}, Franco Belosi³, Antonio Tovar-
6 Sánchez⁷, Araceli Rodriguez-Romero⁷, Gianni Santachiara³, Cécile Guieu⁵, and Karine Sellegri¹

7 ¹ Université Clermont Auvergne, CNRS, Laboratoire de Météorologie Physique (LaMP) F-63000 Clermont-Ferrand, France

8 ² GEOMAR, Helmholtz Centre for Ocean Research Kiel, 24105 Kiel, Germany

9 ³ Institute of Atmospheric Sciences and Climate, National Research Council, 40129 Bologna, Italy

10 ⁴ Mediterranean Institute of Oceanography, 163 avenue de Luminy, Marseille, France

11 ⁵ CNRS, Sorbonne Université, Laboratoire d'Océanographie de Villefranche, UMR7093, Villefranche-sur-Mer

12 ⁶ Marine Biology Research Division, Scripps Institution of Oceanography, 92037 La Jolla, US

13 ⁷ Department of Ecology and Coastal Management, Institute of Marine Sciences of Andalusia (ICMAN-CSIC), 07190 Puerto
14 Real, Spain

15 Correspondence to: K.Sellegri@opgc.cnrs.fr

16 **Abstract.** Ice nucleating particles (INP) have a large impact on the climate-relevant properties of clouds over the oceans.
17 Studies have shown that sea spray aerosols (SSA), produced upon bursting of bubbles at the ocean surface, can be an
18 important source of marine INP, particularly during periods of enhanced biological productivity. Recent mesocosm
19 experiments using natural seawater spiked with nutrients have revealed that marine INP are derived from two separate
20 classes of organic matter in SSA. Despite this finding, existing parameterizations for marine INP abundance are based solely
21 on single variables such as total organic carbon (TOC) or SSA surface area, which may mask specific trends in the separate
22 classes of INPs. The goal of this paper is to improve the understanding of the connection between ocean biology and marine
23 INP abundance by reporting results from a field study and proposing a new parameterization of marine INP that accounts for
24 the two associated classes of organic matter. The PEACETIME cruise took place from May 10 to June 10, 2017 in the
25 Mediterranean Sea. Throughout the cruise, INP concentrations in the surface microlayer (SML) and in SSA produced using a
26 plunging aquarium apparatus were continuously monitored while surface seawater (SSW) and SML biological properties
27 were measured in parallel. The organic content of artificially generated SSA was also evaluated. A dust wet deposition event
28 that occurred during the cruise increased the INP concentrations measured in the SML by an order of magnitude, in line with
29 increases of iron in the SML and bacterial abundances. Increases of INPs in marine SSA (INP_{SSA}) were not observed before
30 a delay of three days compared to increases in the SML, and are likely a result of a strong influence of bulk SSW INP for the
31 temperatures investigated ($T = -18^{\circ}C$ for SSA, $T = -16^{\circ}C$ for SSW). Results confirmed that INP_{SSA} are divided into two classes
32 depending on their associated organic matter. Here we find that warm ($T \geq -22^{\circ}C$) INP_{SSA} concentrations are correlated with
33 water soluble organic matter in the SSA, but also to SSW parameters (POC_{SSW} $INP_{SSW,-16^{\circ}C}$) while cold INP_{SSA} ($T < -22^{\circ}C$)
34 are correlated with SSA water-insoluble organic carbon (WIOC) and SML dissolved organic carbon (DOC) concentration. A
35 relationship was also found between cold INP_{SSA} and SSW microphytoplankton cell abundances, indicating that these
36 species might be at the origin of water insoluble organic matter with surfactant properties and specific IN properties. Using
37 these results, we propose a two-component parameterization for the abundance of INP in marine SSA and compare it with
38 previous single-component models based on SSA surface area and TOC content. This new, two-component parameterization
39 should improve attempts to incorporate marine INP emissions into numerical models. Future studies will be conducted to
40 confirm if our parameterization can be extended to regions of higher biological productivity, such as the Southern Ocean.



41 1 Introduction

42 Ice nucleating particles are a subset of aerosol particles that are required for the heterogeneous nucleation of ice particles in
43 the atmosphere. While extremely rare (Rogers et al., 1998), INP greatly control the ice content of clouds, which is crucial to
44 a range of climate-relevant characteristics including precipitation onset, lifetime, and radiative forcing (Verheggen et al.,
45 2007). Despite their importance, the knowledge of INP sources and concentrations, particularly in marine regions, remains
46 low as evidenced by the large uncertainties in modelled radiative properties of clouds (McCoy et al., 2015; McCoy et al.,
47 2016; Franklin et al., 2013).

48 While the ice nucleating (IN) ability of marine SSA particles is less efficient than their terrestrial counterparts (DeMott
49 et al., 2016), modelling studies have shown that marine INP are of particular importance in part due to the lack of other INP
50 sources in such remote regions (Burrows et al., 2013; Vergara-Temprado et al., 2017). For this reason, recent studies have
51 been conducted to better understand which SSA particles contribute to the marine INP population as well as the relationship
52 between SSA emission and ecosystem productivity. Results from these studies suggest that the IN ability of SSA is linked to
53 the biological productivity of source waters, with higher productivity leading to greater IN activity (DeMott et al., 2016;
54 Bigg, 1973; Schnell and Vali, 1976). For example, it has been shown that both the cell surface and organic exudate of the
55 marine diatom *Thalassiosira pseudonana* can promote freezing at conditions relevant to mixed-phase clouds (Knopf et al.,
56 2011)(Wilson et al., 2015). More recently, mesocosm studies on phytoplankton blooms using two separate in-lab SSA-
57 generation techniques have furthered the understanding of the connection between ocean biology and the IN activity of SSA
58 (McCluskey et al., 2017). In-depth chemical analysis of the artificially generated SSA during this set of experiments has
59 revealed marine INP may be related to two classes of organic matter: a regularly occurring surface-active molecule type
60 related to DOC and long-chain fatty acids, and an episodic heat-labile microbially-derived type (McCluskey et al., 2018a).

61 As the understanding of the connection between ocean biology and marine INP has improved, parameterizations for
62 predicting marine INP abundance using readily available ocean parameters have been proposed. Wilson and co-authors
63 (Wilson et al., 2015) identified a temperature-dependent relationship between TOC and ice nucleating entities (INE) number
64 concentrations in the SML from samples collected in the North Atlantic and Arctic ocean basins. They then extended this
65 relationship from the ocean to the atmosphere to predict the abundance of INP in SSA based on model estimates of marine
66 organic carbon aerosol concentrations. The parameterization was tested for the first time on field measurements of marine
67 aerosol over the North Atlantic at Mace Head and was found to overestimate INP abundance in pristine marine aerosol by a
68 factor of 4 to 100 at -15C and -20C (McCluskey et al., 2018b). In the same study, a new parameterization based on SSA
69 surface area and temperature was proposed (McCluskey et al., 2018b). However, this parameterization did not incorporate
70 the recently observed heat labile organic INPs. Most recently, this parameterization was compared with observations of INP
71 over the Southern Ocean, showing reasonable agreement between predictions and observations at -25C (McCluskey et al.,
72 2019).

73 Despite the recent progress made in the understanding of marine INP, there remains much room for improvement. To
74 date, previous parameterizations have only been tested in the two field studies mentioned in the previous paragraph,
75 underscoring the need for more real-world observations. Furthermore, the field studies conducted so far have taken place in
76 regions of the ocean where biological productivity is high (i.e., North Atlantic and Southern Ocean). As modelling work has
77 shown that the link between ocean biology and SSA organic content properties in oligotrophic waters differs from those in
78 highly productive regions (Burrows et al., 2014) there is need for more measurements in waters with low primary
79 productivity. Finally, despite the finding that marine INP may exist as two separate populations, no model has yet been
80 proposed to account for this.

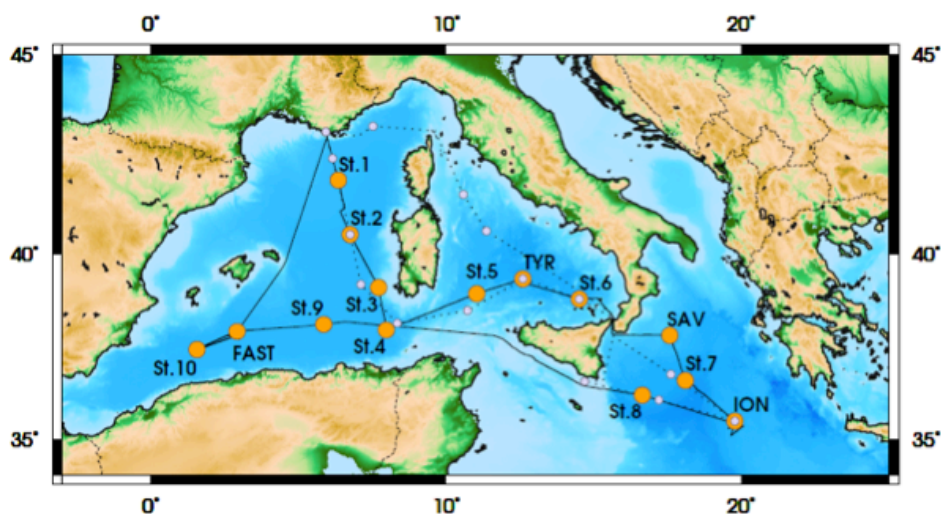
81 This paper addresses the current gaps in the knowledge of marine INP by 1) testing existing parameterizations of INP on
82 a new set of field measurements by extending the current inventory of field measurements beyond eutrophic waters to more



83 oligotrophic regions for the first time 2) improving the understanding of how INPs in the SML and SSA are linked to both
84 seawater biological and SSA organic properties and 3) proposing a new parameterization based on the two-component nature
85 of INPs. Here we present results from the research cruise entitled the ProcEss studies at the Air-sEa Interface after dust
86 deposition in the Mediterranean Sea (PEACETIME) study. The cruise took place in the central and western Mediterranean
87 Sea from May 10-June 10, 2017. Observations of INP concentrations both in the SML and SSA were compared with a suite
88 of surface seawater, surface microlayer, and SSA properties to better determine how INP concentrations were related to
89 biology.

90 2 Methods

91 In the frame of the PEACETIME project (<http://peacetime-project.org/>), an oceanographic campaign took place aboard
92 the French R/V ‘Pourquoi Pas?’ between May 10-June 10, 2017. The purpose of the voyage was to investigate the processes
93 that occur at the air-sea interface in the Mediterranean Sea. Figure 1 shows the transect of the cruise, which started in La
94 Seyne, France and travelled in a clockwise fashion from 35° to 42° latitude and 0° to 20° longitude. The observations and
95 process studies performed on board both in the whole water column and the atmosphere are described elsewhere (Gueiu et
97 al., 2020). Here, we focus on the measurements conducted to describe the SML, SSW, and aerosol properties.



100 Figure 1. Transect of the PEACETIME cruise (May 10 – June 10, 2017).

101 2.1 Surface Seawater (SSW)

102 SSW properties presented here were obtained from sampling at depth of 20 cm and 5 m. First, 21 parameters including
103 various chemical properties, microbial assemblages, hydrological properties, and optical properties were monitored using the
104 ship’s underway system that continuously collected seawater at 5 m under the ship using a large peristaltic pump (Verder
105 VF40 with EPDM hose). These measurements included counts of specific microbial classes (e.g., *Synechococcus*,
106 *Prochlorococcus*, picoeukaryotes, nanoeukaryotes, microphytoplankton, high phycoerythrin containing cells,
107 coccolithophores, cryptophytes), as well as seawater biovolume, chlorophyll-*a* (chl-*a*), and POC concentrations. Chl-*a* was
108 determined from the particulate absorption spectrum line-height at 676 nm after adjusting to PEACETIME chl-*a* from
109 HPLC. POC was estimated from the particulate attenuation at 660 nm using an empirical relationship specific to
110 PEACETIME ($POC = 1405.1 \times c_p(660) - 52.4$). For enumeration of phytoplankton cells, an automated Cytosense flow



111 cytometer (Cytobuoy, NL) operating at a time resolution of one-hour was connected to the continuous underway seawater
112 system. Particles were carried in a laminar flow filtered seawater sheath fluid and subsequently detected with forward scatter
113 (FWS) and sideward scatter (SWS) as well as fluorescence in the red (FLR > 652 nm) and orange (FLO 552-652 nm).
114 Distinction between highly concentrated picophytoplankton and cyanobacteria groups and lower concentrated nano- and
115 microphytoplankton was accomplished using two trigger levels (trigger level FLR 7.34 mV, sampling speed of $4 \text{ mm}^3 \text{ s}^{-1}$
116 analysing $0.65 \pm 0.18 \text{ cm}^3$ and trigger level FLR 14.87 mV at a speed of $8 \text{ mm}^3 \text{ s}^{-1}$ analysing $3.57 \pm 0.97 \text{ cm}^3$).

117 The second set of SSW measurements were made on seawater collected at ~20 cm depth from a pneumatic boat that
118 was periodically deployed at a distance of 2 km from the R/V to avoid contamination. The SSW was manually collected
119 using acid cleaned borosilicate bottles. From these discrete samples, microbial composition and cell abundance of the SSW
120 was monitored as described in a companion paper (Tovar-Sanchez et al., 2019). Measurements included heterotrophic
121 bacteria counts, total non-cyanobacteria like cells (NCBL), cyanobacteria like cells (CBL), and total phytoplankton
122 concentration (NCBL+CBL). These were further segregated into size classes of small, medium, large which roughly
123 correspond to the pico-, nano-, and micro- size classifications for the underway measurements. Trace metals (i.e., Cd, Co,
124 Cu, Fe, Ni, Mo, V, Zn, Pb) were analysed by ICP-MS, although here we only report on Fe. Finally dissolved organic carbon
125 (DOC) and marine gel-like particles, including abundance of transparent exopolymer particles (TEP) and Coomassie
126 stainable particles (CSP) were also measured as described in literature (Engel, 2009).

127 2.2 Surface Microlayer

128 At the same time SSW samples were manually collected on the pneumatic boat, SML samples were also collected using
129 a glass plate sampling method which has been previously described in the literature (Tovar-Sanchez et al., 2019). The glass
130 plate was cleaned overnight with acid and rinsed with ultrapure MQ water. Roughly 100 dips of the glass were conducted to
131 collect 500 mL of SML water into 0.5L acid cleaned low-density polyethylene plastic bottles. The samples were then
132 acidified on board to $\text{pH} < 2$ with ultrapure-grade HCL in a class-100 HEPA laminar flow hood. The same measurements
133 done for the SSW samples (see above) were then made on the SML samples.

134 In addition to biological measurements, concentrations of immersion freezing mode INP in SML samples were
135 measured between May 22-June 7 using the method described previously (Stopelli et al., 2014). Briefly, prior to acidification
136 of the SML samples, additional aliquots were separated and stored in Corning Falcon 15 mL conical tubes and frozen at -
137 20C until analysis. Before INP measurement, each aliquot was gradually defrosted and distributed into an array of 26
138 Eppendorf tubes filled up to 200 μL . The array was then immersed inside an LED based Ice Nuclei Detection Apparatus
139 (LINDA) and the number of ice nucleating particles per liter (INP/L) of SML water was calculated using the method
140 described in a previous report (Vali, 1971).

141 2.3 Artificially Generated Sea Spray Aerosol

142 Sea spray aerosols were generated using a sea spray generation apparatus which has been described previously (Schwier
143 et al., 2015). The apparatus consisted of a 10 L glass tank with a plunging jet system. A continuous flow of seawater
144 collected at 5 m depth using the ship's underway seawater circulating system (described above) was supplied to the
145 apparatus. Particle free air was passed perpendicular to the water surface at a height of 1 cm to send a constant airflow across
146 the surface of the water. Aerosols were then either dried with a 1 meter long silica dryer for online instrumentation (DMPS,
147 CPC, and ACSM), with a 30 cm silica gel dryer cascade impactor sampling with subsequent chemical analysis, or were
148 sampled directly from the sea spray generator onto filters for INP analysis.



149 2.3.1 Size Distribution Measurements

150 Particle size distribution and number concentrations of aerosols generated with the plunging apparatus were
151 monitored using a custom-made differential mobility particle sizer (DMPS) preceded by a 1 micron size-cut impactor and X-
152 ray neutralizer (TSI inc.). Total counts from the DMPS system were checked using a condensation particle counter (CPC,
153 TSI3010). Using the DMPS, a total of 25 size bins ranging between 10-500nm were scanned over a 10-minute time period.
154 For the purpose of the present study, surface area of SSA particles were calculated from the number size distributions.

155 2.3.2 Offline PM1 filter analysis

156 Aerosol particles were also sampled onto PM1 quartz fiber filters mounted on a 4-stage cascade impactor (10 LPM)
157 on a daily basis (24 hour duration). Samples were then extracted in MilliQ water by sonication for 30 minutes for the
158 analysis of water-soluble components. Main inorganic ion abundance (i.e., SO_4^{2-} , NO_3^- , NH_4^+ , Na^+ , Cl^- , K^+ , Mg^{2+} , Ca^{2+}) was
159 analysed via ion chromatography. An IonPac CS16 3x 250 mm Dionex separation column with gradient MSA elution was
160 used for cations, while an IonPac AS11 2 x 250 mm Dionex column with gradient KOH elution was used for anions.
161 Organic content (WSOC and WIOC) were also determined. WSOC was determined using a TOC thermal combustion
162 analyser (Shimadzu TOC-5000A). Total carbon (TC) content was measured on filter punches which were cut prior to water
163 extraction using a thermal combustion analyser equipped with a furnace for solid samples (Analytik Jena, Multi NC2100S).
164 Prior to analysis, the filter punches were acidified to remove inorganic carbon from TC to obtain TOC.

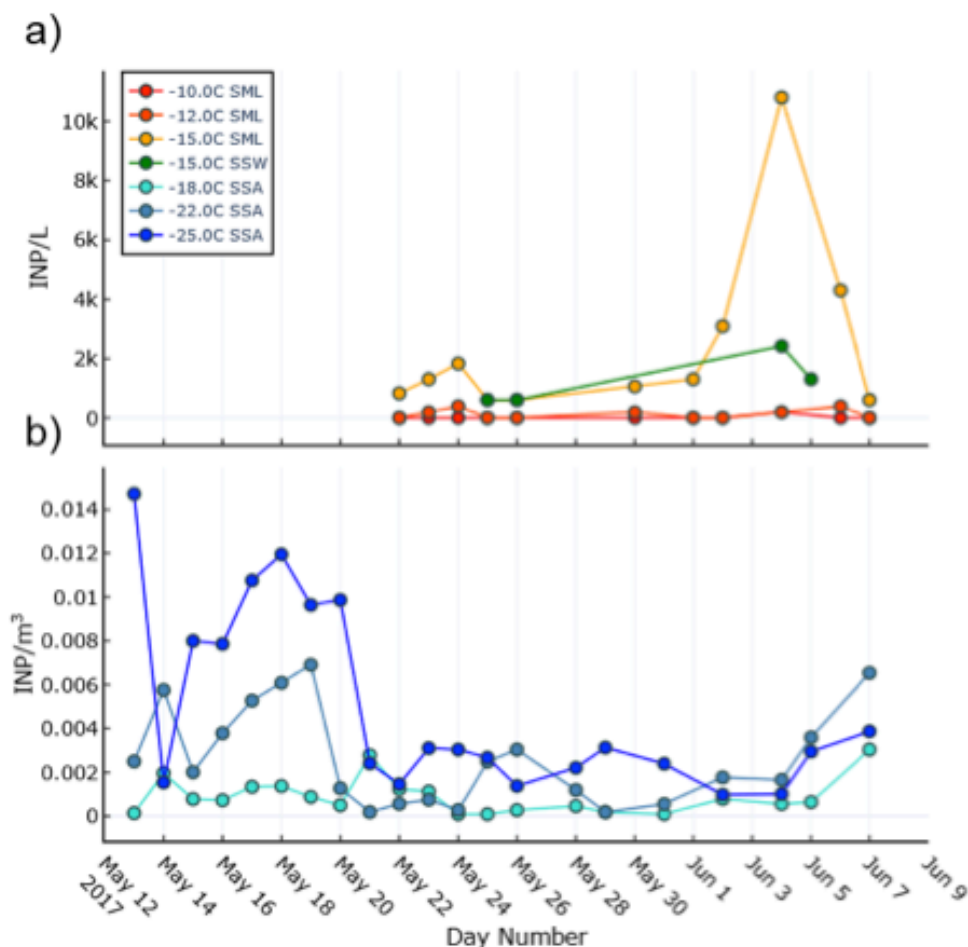
165 2.3.3 INPs

166 INP concentrations were determined from filter-based samples of total suspended particles over a 24h duration daily or
167 from the average of two filters (day and night). The concentration of INPs in the SSA was determined for the condensation
168 freezing mode using a Dynamic Filter Processing Chamber (DFPC). Briefly, SSA formed using the aquarium apparatus were
169 impacted onto 47mm nitrocellulose filters which were then placed on a metal plate coated with a smooth surface of Vaseline.
170 Air entered the chamber and was sent through a cooling coil allowing it to become saturated with respect to ice. Different
171 supersaturations with respect to ice and water were obtained by controlling the temperatures of the filter and the air flowing
172 across the filter. Filter air temperature combinations were set three different ways, all set to a supersaturation with respect to
173 water of 1.02. The filter temperatures were -18, -22, and -25C (-15.9, -19.6, and -22.3 C for air temperature). Filters were
174 placed inside the DFPC for 15 minutes and monitored for formation of ice crystals upon activation of INPs. Based on
175 sampling time and flow rate, the number of INP/volume were calculated.

176 3 Results

177 3.1 INP in SML and SSA

178 Ice nucleating particle concentrations were determined for the SSW, SML and SSA. Figure 2a shows the concentration
179 of INP in the SML (INP_{SML}) at three different temperatures and in the SSW (INP_{SSW}) at -15.0C as monitored using the
180 LINDA instrument. In the SML, the trends between the three temperatures are similar, although with decreasing abundances
181 at warmer temperatures to the point that INP at $T=-10\text{C}$ were rarely observed. An initial increase occurred on May 24
182 (1.8×10^3 INP/L at $T=-15\text{C}$) followed by a much larger peak around June 4th (1.1×10^4 INP/L at $T=-15\text{C}$). SSW concentrations
183 were similar to SML concentrations, with the exception of June 4 when SML INP became enriched relative to the SSW.



186 **Figure 2.** INP concentrations observed during the PEACETIME cruise. a) INP_{SML} and INP_{SSW} concentration as measured using
187 the LINDA instrument and b) INP_{SSA} concentrations observed by the DFPC.

188 Figure 2b shows the concentration of ice nucleating particles in SSA (INP_{SSA}) at three different temperatures as
189 observed by the DFPC. It should be noted that INP_{SSA} measurements were conducted at colder temperatures than for the
190 INP_{SML} measurements due to differences between the LINDA and DFPC instruments. In general, the largest concentrations
191 of INP_{SSA} were observed at the beginning of the voyage between May 12-May 20. For example, INP_{SSA,-25C} peaked on May
192 12 (14.7×10^{-3} INP/m³) and again on May 18 (11.9×10^{-3} INP/m³). After May 20, a considerable drop in INP_{SSA,-25C}
193 concentrations was observed. Concentrations remained at this level, albeit with slight fluctuations, before increasing again
194 between June 5-7 to a second peak of 3.9×10^{-3} INP/m³ on June 7. Both INP_{SML} and INP_{SSA} showed increases during June
195 after a rain event during which iron became highly enriched in the SML as a result of dust deposition (see next section).
196 Interestingly, the peak in INP_{SSA} during this time occurred one day after the increase observed for INP_{SML}.

197 3.2 Correlations between INP and Biogeochemical Conditions

198 As described in the methods section, various seawater biogeochemical properties were monitored throughout the voyage
199 for the SSW and SML. Plots of selected continuous measurements from the R/V's underway sampling system and discrete
200 measurements from the pneumatic boat of relevant biogeochemical values are found in the supporting information (SI)
201 (Figure S1 and Figure S2, respectively). Biogeochemical properties are described in more detail in our companion papers



202 (Guieu et al., 2020; Tovar-Sanchez et al., 2019) and gel properties will be discussed in an upcoming paper. Here, we present
 203 a broad summary. In general, surface waters were characterized by oligotrophic conditions as expected for the season.
 204 Bacteria concentrations ranged between 2×10^5 and 7×10^5 cells/mL in the SSW and were greatest at the start and end periods
 205 of the voyage. NCBL abundance followed a similar trend and ranged between 400-4000 cells/mL. DOC and POC values
 206 were within the range of expected values for the oligotrophic Mediterranean (Pujo-Pay et al., 2011), with DOC ranging
 207 between 700-900 $\mu\text{gC/L}$ and POC between 42-80 $\mu\text{gC/L}$. SSW TEP concentrations ranged between 1.2×10^6 and 1.1×10^7
 208 particles/L, with CSP between 5.6×10^6 and 9.3×10^6 particles/L, and will be discussed in a future paper.

209 Enrichment factors in the SML relative to the SSW remained low with an average of 1.10 for DOC, 1.07 for bacteria,
 210 and 1.17 for NCBL. As POC was not measured in the SML, we cannot report the EF. TEP was typically enriched relative to
 211 the SSW, with an average EF of 4.5, while CSP EF was on average 2.7. Of importance, a dust deposition event occurred on
 212 June 4 leading to a drastic increase in SML dissolved iron relative to the SSW (EF ~ 800). This deposition event had
 213 important impacts on the biology of the surface seawaters, which is the focus of another paper (Guieu et al., 2020). As a
 214 result, TEP EF increased to 17, bacteria EF increased to 1.5, and NCBL to 2.4. We next discuss the correlations between INP
 215 abundance and biogeochemical properties in the following sections.

216 3.2.1 Correlations Between INP_{SML} Abundance and Seawater Properties

217 **Table 1. Correlations between $\text{INP}_{\text{SML},-15\text{C}}$ and seawater properties.**

Variable	p	R (R^2)	n
SSW			
DOC	0.045	-0.76 (0.59)	7
CSP _{abundance}	0.005	0.87 (0.75)	8
Nanoeukaryotes $<10\mu\text{m}$	0.04	-0.63 (0.40)	11
SML			
Dissolved Iron	2.0×10^{-6}	0.99 (0.98)	8
TEP EF	0.0003	0.95 (0.90)	8
Total Bacteria EF	0.0007	0.93 (0.87)	8
CSP _{abundance}	0.005	0.87 (0.76)	8
Total NCBL	0.005	0.87 (0.75)	8
pico NCBL	0.009	0.84 (0.71)	8
Total bacteria	0.02	0.81 (0.65)	8
Phytoplankton (NCBL+CBL)	0.02	0.78 (0.61)	8
NCBL EF	0.78	0.78 (0.61)	8
DOC EF	0.04	0.78 (0.60)	7
nano NCBL	0.03	0.77 (0.59)	8

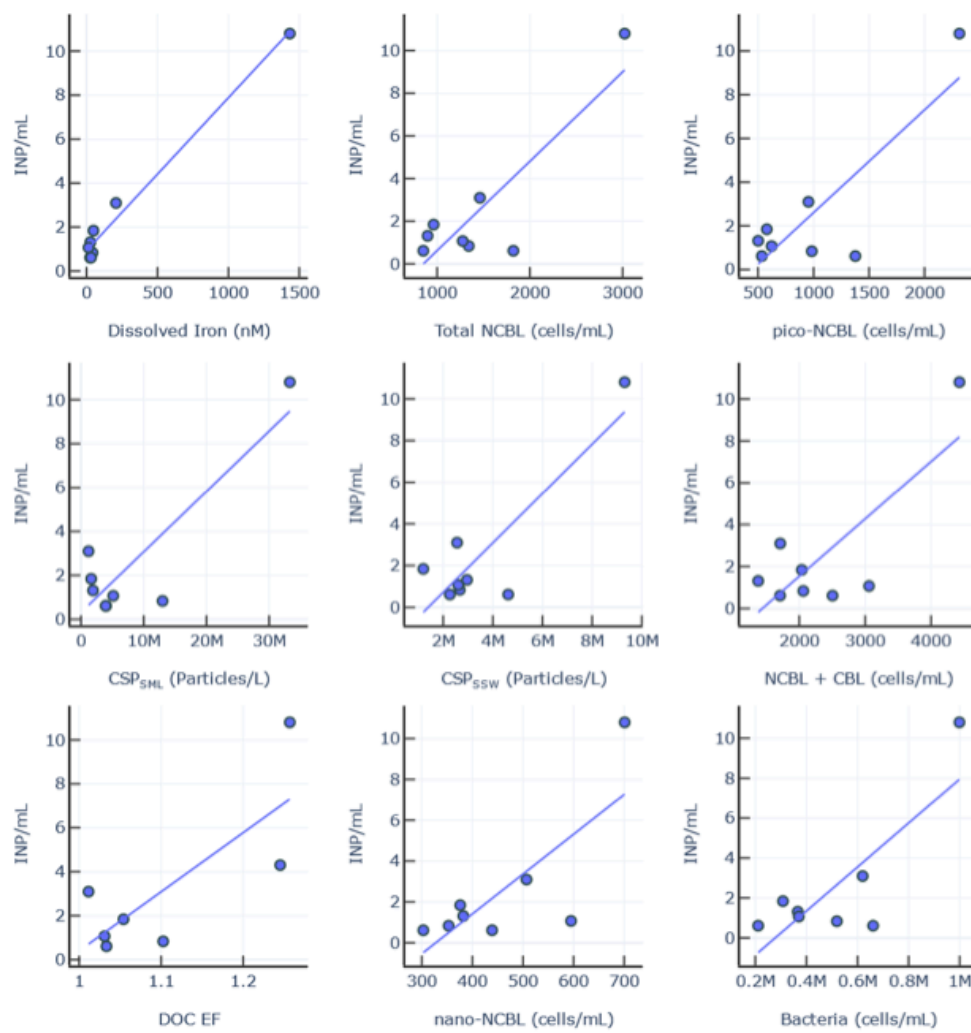
218
 219 Table 1 shows the statistically significant correlations ($p < 0.05$) between $\text{INP}_{\text{SML},-15\text{C}}$ and observed seawater
 220 properties. We note the only statistically significant correlations between $\text{INP}_{\text{SML},-15\text{C}}$ and SSW parameters were with DOC
 221 ($R=-0.76$, $n=7$), CSP ($R=0.87$, $n=8$), and nanoeukaryote cell abundance $<10\mu\text{m}$ ($R=-0.63$ $n=11$) as measured from the
 222 underway system. Nanoeukaryote cell abundances in the SSW were identified in a companion paper (Freney et al., this
 223 issue) as related to a fraction of organic matter that has a signature of fatty acids and amino acids (MOA), likely enriched in
 224 the SML and having surface active properties. Figure 3 shows scatterplots of relationships with significant correlations. In
 225 the SML, $\text{INP}_{\text{SML},-15\text{C}}$ were most strongly positively correlated with dissolved iron. However, this relationship as well as
 226 others, may be skewed by an outlier due to the dramatic increase in iron observed on June 4 (Figure S2a) as described
 227 previously. Indeed, when days after June 3 are removed, only the relation to Fe_{SML} ($R=0.91$, $p=0.01$ $n=6$) and bacteria HnA
 228 (high nucleic acid) in the SSW ($R=0.83$, $p=0.04$, $n=6$) remain as significant positive correlations. This suggests that the dust
 229 deposition event observed during June had a significant impact on the $\text{INP}_{\text{SML},-15\text{C}}$ concentration. The strong correlation with
 230 Fe_{SML} indicates that the presence of dust in the SML, of which Fe_{SML} is a tracer, may increase the $\text{INP}_{\text{SML},-15\text{C}}$ concentrations,



231 as dust is known to have good INP properties. The correlations with biological populations found in the SML of all types
232 (NCBL ($R=0.77$), pico NCBL ($R=0.84$), nano NCBL ($R=0.77$), total heterotrophic bacteria ($R=0.81$), and total
233 phytoplankton (NCBL and CBL combined) ($R=0.78$) cell counts) suggests that some of the biological species found in these
234 groups and developed over the dust particles also have good INP properties. It is difficult from this data set to segregate
235 between the dust and biological impact on the $INP_{SML,-15C}$.

236 Previous reports examining the correlation between INP and microbial abundance have yielded mixed results. For
237 example, a report of INP in Arctic SML and SSW found no statistically significant relationship between the temperature at
238 which 10% of droplets had frozen and bacteria or phytoplankton abundances in bulk SSW and SML samples (Irish et al.,
239 2017). However, recent mesocosm studies using nutrient-enriched seawater found that INP abundances between $-15C$ and $-$
240 $25C$ in the aerosol phase were positively correlated with aerosolized bacterial abundance (McCluskey et al., 2017).

242



243

244 **Figure 3.** Correlation matrix of INP in the SML ($INP_{SML,-15C}$) and various biogeochemical parameters.



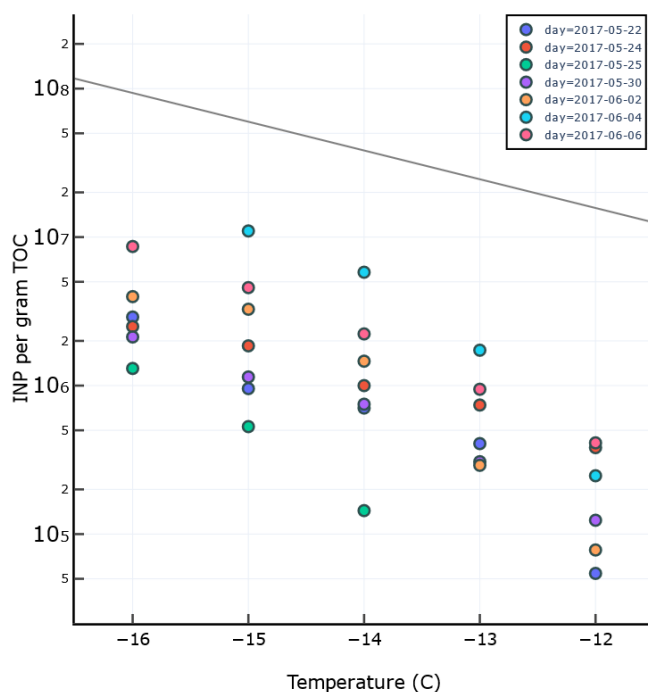
245

246 Neither POC in the SSW (POC_{SSW}) nor DOC in the SML (DOC_{SML}) was significantly correlated with $INP_{SML,-15C}$
247 ($R=-0.35$, $p=0.29$, $n=11$, and $R=0.37$, $p=0.42$, $n=7$ respectively). Interestingly, DOC EF was significantly correlated with
248 $INP_{SML,-15C}$ ($R=0.78$, $p=0.04$, $n=7$), again due to the dust event. This indicates that the fraction of DOC which is enriched in
249 the SML during the dust event has specific IN properties. This DOC type enriched in the SML is likely connected to the CSP
250 abundance, albeit not to the TEP.

251

252 A previous study by Wilson and co-authors presented an INP parameterization (hereafter termed W15) based on a
253 positive relationship between seawater TOC and INP abundance in Arctic, North Pacific, and Atlantic SML and SSW waters
254 (Wilson et al., 2015). Total organic carbon (TOC $\mu\text{gC/l}$), derived here as the sum of particulate organic carbon in the SSW
255 (POC_{SSW}) and dissolved organic carbon in the SML (DOC_{SML}), was weakly correlated with $INP_{SML,-15C}$ ($R=0.31$, $p=0.49$,
256 $n=7$). Figure 6 shows the observed $INP_{SML,-15C}/\text{TOC}$ ratio (INP per gram of OC) in the SML for various temperatures and
257 days of the experiment compared with the W15 parameterization (grey line). Our results show observed INP_{SML}/TOC ratios
258 below those expected by the model proposed by W15, indicating the TOC in Mediterranean waters is less IN active at these
259 temperatures than predicted by the W15 parameterization.

260 In agreement with our findings, a recent study found that the W15 model over-predicted observed INP
261 concentrations in the aerosol phase during two separate mesocosm experiments (McCluskey et al., 2017) by assuming the
262 INP/TOC ratio in the SML was preserved in the aerosol phase. The authors of that study speculated that the overprediction
263 by the W15 model was due to the fact that it does not account for the complex transfer mechanism of organic matter from
264 the SML to the aerosol phase. Our results here show that the overprediction by W15 persists even when calculating INP in
265 the SML and therefore the overprediction may be due to other factors beyond the transfer of organic matter from the SML to
266 the atmosphere. We stress however, that the TOC value used in this study was derived using DOC_{SML} and POC_{SSW} values as
267 POC measurements in the SML were not conducted. There typically exists an enrichment of organic matter in the SML
268 relative to the bulk seawater. It is thus possible that the POC_{SSW} we used to calculate TOC was below the actual POC content
269 in the SML, thus underestimating TOC. However, if this were the case, a higher abundance of TOC would only further
270 increase the overprediction of W15 relative to our observations.





271 **Figure 4. Observed INP/TOC ratio during PEACETIME experiment for different temperatures. The gray line is a model fit from**
272 **Wilson et al., 2015.**

273 Another possible explanation for the discrepancy between our results and those from W15 is that the oligotrophic
274 nature of Mediterranean waters results in a TOC of a different chemical composition than what is observed in more
275 biologically productive waters such as the Arctic and Atlantic. For example, the pool of TOC during this study was
276 dominated by DOC and featured low POC content, presumably due to low biological productivity.

277

278 In summary, $INP_{SML,-15C}$ increased with SML microbial cell counts (e.g., NCBL and heterotrophic bacteria), Fe_{SML}
279 and DOC_{EF} during a dust deposition event, but were overall not correlated with TOC nor DOC. Compared to previous
280 studies, the INP/TOC observed here is low. We surmise that the overprediction of INP/TOC by the model may either be
281 caused by a different relationship between INP and TOC at warmer temperatures, or possibly due to the chemical
282 characteristics of TOC in the oligotrophic Mediterranean. This complicated relationship between seawater OC and INP_{SML}
283 highlights the need for further studies focused on the chemical composition of DOC and POC in bulk SSW and SML.
284 Further experiments during low and high biological productivity are needed in controlled environments to better determine
285 under what conditions (oligotrophic and eutrophic) and location in the water column (i.e., bulk SSW vs SML) TOC, bacteria,
286 and phytoplankton are linked to INP across a range of temperatures. The impact of dust deposition on $INP_{SML,-15C}$ is fairly
287 large, as we observe an increase of $INP_{SML,-15C}$ by almost an order of magnitude during the dust event. This impact could
288 have climate implications if $INP_{SML,-15C}$ were efficiently transferred to the sea spray emitted to the atmosphere.

289 3.2.2 Correlations Between INP_{SSA} Abundance and Observed SSA and Seawater Conditions

290 In the following section, we compare INP_{SSA} at various temperatures with seawater and SSA properties. For
291 comparison with seawater properties, INP_{SSA} was first normalized by SSA particle surface area ($SSA_{diam=10-500nm}$) (Figure
292 S3). As total particle counts matched quite well with SSA counts between 10-500 nm diameter, and as most of the surface
293 area of sea spray is comprised between this size range, this value is a reasonable estimate of total SSA particle surface area.
294 Submicron particle concentrations ranged between 1000-3000 particles/cm³ (Figure S4) and its dependence of seawater
295 biology is further explored in a separate manuscript. Interestingly, despite the fluctuations, no statistically significant
296 correlations were seen between total submicron particle counts or total SSA surface area and INP_{SSA} at all three temperatures
297 (Figure S5a,b).

298 Figure 5 shows the scatter plots between $INP_{SSA,-18C}$ normalized by SSA particle surface area ($SSA_{diam=10-500nm}$)
299 and conditions in the SSW as well as scatter plots between non-normalized $INP_{SSA,-18C}$ and non-normalized SSA properties,
300 for relationships that were found significant. Corresponding correlation parameters are reported Table 2. Correlations did
301 not differ significantly when performed over the whole data set or when performed over a smaller data set that excludes the
302 dust wet deposition event. Surprisingly, there was no significant correlation between $INP_{SSA,-18C}$ and conditions in the SML,
303 including TEP and CSP abundance and enrichment factors, bacteria abundance and enrichment factors, nor with INP_{SML} as
304 measured by the LINDA instrument. This is somewhat unexpected considering INP in the SML at -15C was correlated with
305 SML bacteria counts, which are expected to transfer efficiently from the SML to the aerosol phase, an assumption widely
306 used in the modelling community. Table 2 does however show that $INP_{SSA,-18C}$ are significantly correlated with POC_{SSW}
307 ($R=0.71$, $p=.002$, $n=16$) and $INP_{SSW,-16C}$. This could indicate that INP at this temperature come from the bulk water rather
308 than the SML. We also note that while a correlation exists with $INP_{SSW,-16C}$, with a sample size of $n=4$ this result requires
309 further validation.

310 **Table 2. Correlations for $INP_{SSA,-18C}$ and observed conditions.**

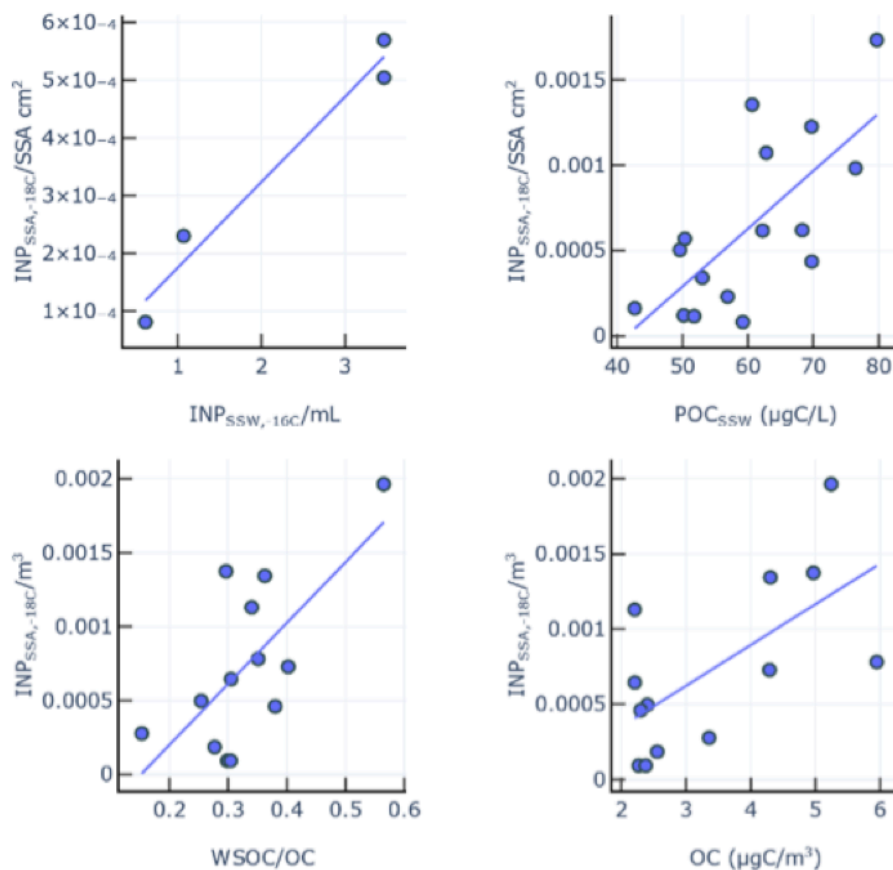
Variable	p	R (R ²)	n
SSW			



$\text{INP}_{\text{SSW},-16}$	0.01	0.99 (0.98)	4
POC	0.002	0.71 (0.50)	16
SSA			
OC	0.02	0.64 (0.41)	13
WSOC/OC	0.01	0.68 (0.47)	13

311

312 Table 2 also shows the significant correlations between $\text{INP}_{\text{SSA},-18\text{C}}$ and SSA properties. A positive correlation exists
 313 between $\text{INP}_{\text{SSA},-18\text{C}}$ and SSA organic carbon (OC) as well as the ratio of SSA water-soluble organic carbon to organic carbon
 314 (WSOC/OC). The correlation between WSOC/OC and $\text{INP}_{\text{SSA},-18\text{C}}$ makes sense given the finding that $\text{INP}_{\text{SSA},-18\text{C}}$ was
 315 correlated with POC_{SSW} , as a higher WSOC/OC value would suggest a higher fraction of soluble organics which would be
 316 expected to transfer to the atmosphere from the bulk SSW rather than the SML due to their high solubility.



319 **Figure 5. Correlation matrix of INP in SSA at -18C and various biogeochemical parameters.**

320 Figure 6 shows the organic content of artificially generated SSA using the plunging aquarium system continuously
 321 filled with seawater from the boat's underway system. SSA organic carbon concentration (OC) was greatest during the first
 322 part of the cruise, decreasing from $\sim 6 \mu\text{gC}/\text{m}^3$ (May 15), down to ~ 2.5 at FAST (June 5), except for a brief increase on May
 323 26 ($3.6 \mu\text{gC}/\text{m}^3$). The highest concentration of OC was concomitant with a bacteria abundance peak in SSW and SML
 324 bacteria and DOC (Figure S2). Interestingly, OC was not enhanced on June 5th despite the enhanced seawater bacteria and



325 DOC concentration around the same time (Figure S2). WIOC peaked on May 15 ($3.9 \mu\text{gC}/\text{m}^3$), May 18 ($3.5 \mu\text{gC}/\text{m}^3$), and
 326 May 26 ($2.8 \mu\text{gC}/\text{m}^3$). A separate manuscript discusses the trend and controls on SSA chemical composition (Freney et al.,
 327 2020).

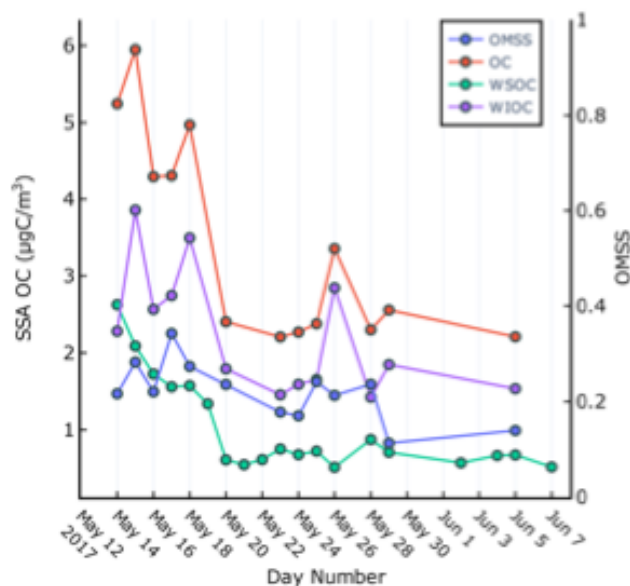


Figure 6. Organic carbon content of SSA.

Figure 7 shows the correlations between $\text{INP}_{\text{SSA},-25\text{C}}$ and properties of SSW, SML and SSA for parameters they were found to be significant. In Table 3 we report the corresponding correlation parameters. At this temperature, INP_{SSA} were significantly correlated with DOC_{SML} , a result not seen for the warmer INP at -18C . We also note that $\text{INP}_{\text{SSA},-25\text{C}}$ was not correlated with DOC_{SSW} , potentially indicating an important step in the process of transfer of IN active DOC material to the atmosphere is its

362 enrichment at the SML. $\text{INP}_{\text{SSA},-25\text{C}}$ was also correlated with SSW concentrations of micro NCBL ($R=0.84$, $p=0.0006$) and
 363 cryptophytes. $\text{INP}_{\text{SSA},-25\text{C}}$ were also correlated to POC_{SSW} ($R=0.53$, $p=0.04$) although with less statistical significance than the
 364 correlation between POC_{SSW} and $\text{INP}_{\text{SSA},-18\text{C}}$. Phytoplankton are known for their ability to produce extracellular polymeric
 365 substances (Thornton, 2014). A previous mesocosm experiment showed microbially-derived fatty acids were efficiently
 366 ejected from the seawater as SSA, increasing the fraction of highly-aliphatic OC (Cochran et al., 2017). Seemingly in
 367 agreement with this, our results show that $\text{INP}_{\text{SSA},-25\text{C}}$ was correlated with SSA WIOC and organic mass fraction of sea spray
 368 (OMSS). To summarize, $\text{INP}_{\text{SSA},-25\text{C}}$ was correlated with DOC_{SML} , larger species of phytoplankton in the SSW, and water
 369 insoluble organic carbon in the SSA.

370 Table 3. Correlations between $\text{INP}_{\text{SSA},-25\text{C}}$ and observed conditions.

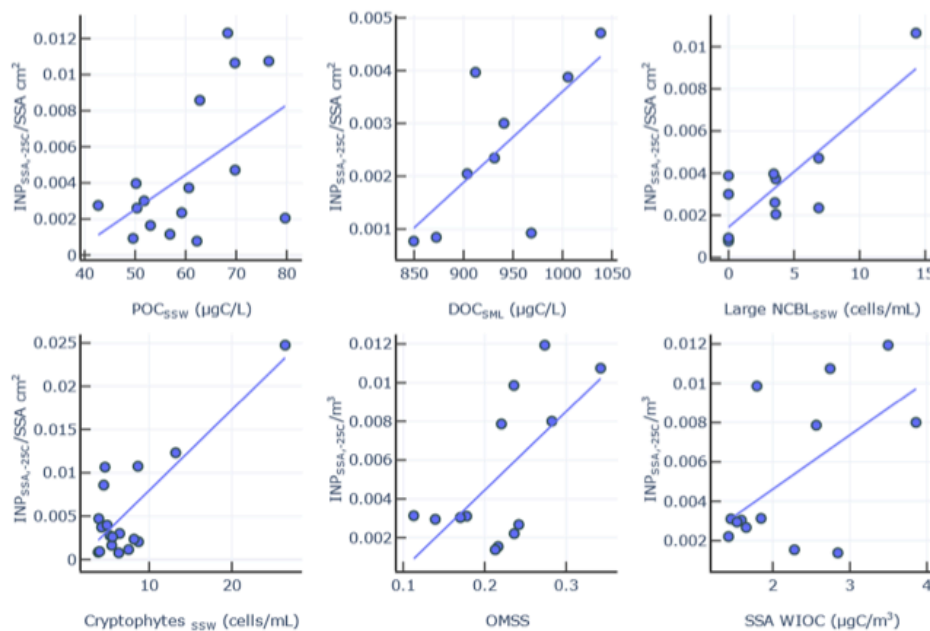
Variable	p	R (R ²)	n
SML			
DOC	0.03	0.70 (0.50)	9
SSW			
micro-NCBL	0.0006	0.84 (0.71)	12
Cryptophytes	0.000017	0.82 (0.67)	19
POC	0.04	0.53 (0.28)	16
SSA			
OMSS	0.02	0.65 (0.42)	13
WIOC	0.04	0.58 (0.34)	13

371
 372 The results presented thus far point towards the existence of two classes of INP with separate sources: 1) a class of
 373 INP related to POC in the bulk SSW and SSA water soluble organic carbon and 2) a class of INP related to large
 374 phytoplankton and POC in the SSW, DOC in the SML, and WIOC in SSA. These findings of a two-component marine INP
 375 population agree with a recent study which also reported on the existence of dual classes of INP emitted as SSA during two



376 mesocosm experiments, described as: 1) particulate organic carbon INPs coming from intact cells or IN-active microbe
 377 fragments and 2) dissolved organic carbon INPs composed of IN-active molecules enhanced during periods when the SML
 378 is enriched with exudates and cellular detritus (McCluskey et al., 2018a). However, in contrast to that study, we report here
 379 the existence of separate temperature regimes at which each INP class is active. Here, the first class of INP consists of INP
 380 that are more active at warmer temperatures ($T = -18\text{C}$). The second class of INP are active at colder temperatures ($T = -$
 381 25C). Interestingly, INP at $T=-22\text{C}$ correlates with items from both warm and cold (Table S1).

383



386 **Figure 7. Correlation matrix of INP in SSA at -25C and various biogeochemical parameters.**

387 **4 Proposal of New INP Parameterization and Comparison with Previous Models**

388 To date, parameterizations for the estimation of INPs in SSA have not incorporated the knowledge of a two-
 389 component INP population. Rather, they have predicted INP based on TOC or SSA surface area (W15 and MC18,
 390 respectively). Here we propose a new, two-component temperature-dependent parameterization that accounts for the two
 391 classes of organic matter that contribute to the total INP population, as discussed in the previous section, to calculate INP per
 392 m^3 per unit SSA surface area. In our model, warm INP ($\geq -24\text{C}$) are linked to POC_{SSW} ($\mu\text{gC/L}$) as shown in Eq. 1, while cold

$$(1) \quad \frac{\text{INP}_{T \geq -22}}{\mu\text{m}^2} = \exp(-35.01 - (.304 * T) + (.056 * \text{POC}))$$

$$(2) \quad \frac{\text{INP}_{T < -22}}{\mu\text{m}^2} = \exp(-29.31 - (.1805 * T) + (.113 * \text{NCBL}_{\text{large}}))$$

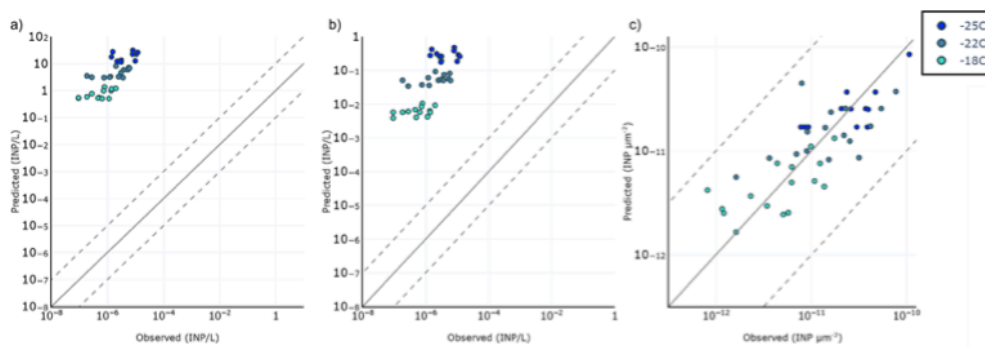
393 INP ($< -24\text{C}$) are linked to the abundance of large NCBL (cells/mL) as shown in Eq. 2:

394 NCBL large were chosen for equation 2 rather than DOC_{SML} due to the difficulty in determining such a variable remotely.
 395 We justify this by noting that the DOC here is likely related to the NCBL as large phytoplankton are known for their ability
 396 to secrete large amounts of extracellular material which become enriched at the SML. We further note that the link between
 397 large NCBL and the class of DOC in the SML that is IN active may change depending on a number of factors (e.g., trophic
 398 status) and thus needs to be verified in future studies.



399 Figure 6 shows the comparison of our new model with the W15 (Figure 6a) and MC18 (Figure 6b)
400 parameterizations. Similar to the comparison between W15's parameterization with seawater INP, a large overprediction
401 occurs relative to our observations. Figure 6b shows that while MC18 is a slight improvement, it still overpredicts INP by
402 four orders of magnitude. Figure 6c shows the use of our two-part model which considers the separate classes of INP and
403 shows good agreement between observations and predictions.

404
406



407 **Figure 8. Different models for INP_{SSA} prediction. a) Wilson model, b) McCluskey, c) our model where INP_{SSA} ≥ -22C are related to**
408 **SSW POC INP < -22C are related to micro NCBL in SSW.**

409 5 Conclusions

410 In this paper we have presented results from the month-long PEACETIME cruise which took place in the Mediterranean
411 Sea during the spring of 2017, which was characterized with a dust wet deposition event that occurred towards the end of the
412 cruise.

413 First, we find that the INP concentrations measured in the SSW are in line with the INP measured in the SML, except
414 during the dust wet deposition event when they are significantly enriched in the SML. In the SML, the increase of INP_{SML,-15C}
415 concentrations during this dust wet deposition event follow the SML microbial cell counts (e.g., NCBL, CBL and
416 heterotrophic bacteria), Fe_{SML} and DOC_{EF}. Excluding this dust event, INP_{SML,-15C} are still correlated, although more
417 moderately, to bacteria and Fe in the SML. Overall INP_{SML,-15C} were not correlated with TOC nor DOC and compared to
418 previous studies, the INP/TOC observed here is low. We surmise that the overprediction of modelled INP/TOC is a result of
419 TOC from the oligotrophic Mediterranean being less IN active.

420 The impact of dust deposition on INP_{SML,-15C} is fairly large, as we observe an increase of INP_{SML,-15C} by almost an
421 order of magnitude during this event. This impact of dust deposition could have climate implications if INP_{SML,-15C} were
422 efficiently transferred to the sea spray emitted to the atmosphere. However, we find that INP_{SSA} does not evolve as the
423 INP_{SML} does. INP_{SSA} are not increased as INP_{SML,-15C} are during the dust event. An increase of INP_{SSA} is observed at least
424 with a three days delay after the dust wet deposition event. This can be due to INP_{SSA} measured at -18°C, (the closest
425 temperature to the ones at which INPSWL and INPSML are measured) being more influenced by the INP concentration in
426 the bulk surface seawater (INP_{SSW,-16C}). It is possible that IN active species deposited during the rain event, either dust-
427 related or biology-related, take a few days before entering the bulk surface layer.

428 In general, we observed the existence of two classes of INP_{SSA}, each linked to different classes of organic matter. Our
429 results indicate each class is active at separate temperatures. Warmer INP (INP_{SSA,-18C}) are linked to water soluble organic
430 matter in the SSA, but also to SSW parameters (POC_{SSW} INP_{SSW,-16C}). This indicates that INP at this temperature come from
431 the bulk water rather than the SML. Colder INP (INP_{SSA,-25C}) are rather correlated with SSA water-insoluble organic carbon,
432 and SML properties (dissolved organic carbon). As the colder INP are correlated to the SSW microphytoplankton cell



433 abundance as well, we hypothesize that these classes of phytoplankton produce surface-active water-insoluble organic matter
434 that is active as IN at these temperatures and are transferred to the atmosphere via the SML. Unfortunately, we do not have
435 measurements of the “colder” temperatures INP in the SML to check this hypothesis.

436 We finally proposed a two-component model for marine INP abundance based on seawater POC and SSW microbial
437 abundance. We then compared this with previous single component models based on SSA surface area and TOC content.
438 Our results should help improve attempts to incorporate marine INP emissions into numerical models. Future studies should
439 be conducted to confirm if our model can be extended to regions of higher biological productivity, such as the Southern
440 Ocean.

441

442 **Acknowledgements** This study is a contribution to the PEACETIME project (<http://peacetime-project.org>), a joint
443 initiative of the MERMEX and ChArMEX components supported by CNRS-INSU, IFREMER, CEA, and Météo-
444 France as part of the programme MISTRALS coordinated by INSU. PEACETIME was endorsed as a process
445 study by GEOTRACES. PEACETIME cruise <https://doi.org/10.17600/17000300>. We thank the captain and the
446 crew of the RV *Pourquoi Pas ?* for their professionalism and their work at sea. The underway optical
447 instrumentation was provided by Emmanuel Boss’s group funded by Nasa Ocean Biology and Biogeochemistry.
448 This work has also received funding from the European Research Council (ERC) under the European Union’s
449 Horizon 2020 research and innovation program (Sea2Cloud grant agreement No 771369). Sea2Cloud was
450 endorsed by SOLAS.

451

452



452

453 **References**

- 454 Bigg, E. K.: Ice Nucleus Concentrations in Remote Areas, *J. Atmos. Sci.*, 30, 1153-1157,
455 [https://doi.org/10.1175/1520-0469\(1973\)030%3C1153:INCIRA%3E2.0.CO;2](https://doi.org/10.1175/1520-0469(1973)030%3C1153:INCIRA%3E2.0.CO;2), 1973.
- 456 Burrows, S. M., Hoose, C., Pöschl, U., and Lawrence, M. G.: Ice Nuclei in Marine Air: Biogenic Particles or Dust?,
457 *ACP*, 13, 245-267, <https://doi.org/10.5194/acp-13-245-2013>, 2013.
- 458 Burrows, S. M., Ogunro, O., Frossard, A. A., Russell, L. M., Rasch, P. J., and Elliott, S. M.: A Physically Based
459 Framework for Modeling the Organic Fractionation of Sea Spray Aerosol from Bubble Film Langmuir
460 Equilibria, *ACP*, 14, 13601-13629, <https://doi.org/10.5194/acp-14-13601-2014>, 2014.
- 461 Cochran, R. E., Laskina, O., Trueblood, J. V., Estillore, A. D., Morris, H. S., Jayarathne, T., Sultana, C. M., Lee, C.,
462 Lin, P., Laskina, J., Laskin, A., Dowling, J. A., Qin, Z., Cappa, C. D., Bertram, T. H., Tivanski, A. V., Stone, E. A.,
463 Prather, K. A., and Grassian, V. H.: Molecular Diversity of Sea Spray Aerosol Particles: Impact of Ocean
464 Biology on Particle Composition and Hygroscopicity, *Chem.*, 2, 655-667,
465 <https://doi.org/10.1016/j.chempr.2017.03.007>, 2017.
- 466 DeMott, P. J., Hill, T. C. J., McCluskey, C. S., Prather, K. A., Collins, D. B., Sullivan, R. C., Ruppel, M. J., Mason, R.
467 H., Irish, V. E., Lee, T., Hwang, C. Y., Rhee, T. S., Snider, J. R., McMeeking, G. R., Dhaniyala, S., Lewis, E. R.,
468 Wentzell, J. J. B., Abbatt, J., Lee, C., Sultana, C. M., Ault, A. P., Axson, J. L., Martinez, M. D., Venero, I.,
469 Santos-Figueroa, G., Stokes, D. M., Deane, G. B., Mayol-Bracero, O. L., Grassian, V. H., Bertram, T. H.,
470 Bertram, A. K., Moffett, B. F., and Franc, G. D.: Sea Spray Aerosol as a Unique Source of ice Nucleating
471 Particles, *PNAS*, 113, 5797-5803, <https://doi.org/10.1073/pnas.1514034112>, 2016.
- 472 Engel, A.: Determination of Marine Gel Particles, in: *Practical Guidelines for the Analysis of Seawater*, edited by:
473 Wurl, O., CRC Press Taylor & Francis Group), Boca Raton, FL, 125-142, 2009.
- 474 Franklin, C. N., Z. Sun, D. B., Yan, M. D. H., and Bodas-Salcedo, A.: Evaluation of Clouds in ACCESS Using the
475 Satellite Simulator Package COSP: Global, Seasonal, and Regional Cloud Properties, *J. Geophys. Res. Atmos.*,
476 118, 732-748, <https://doi.org/10.1029/2012JD018469>, 2013.
- 477 Freney, E., Sellegri, K., Nicosia, A., Trueblood, J. V., Bloss, M., Rinaldi, M., Prevot, A., Slowik, J. G., Thyssen, M.,
478 Gregori, G., Engel, A., Zanker, B., Desboeufs, K., Asmi, E., Lefevre, D., and Guieu, C.: High Time Resolution
479 of Organic Content and Biological Origin of Mediterranean Sea Spray Aerosol, *ACP*, 2020.
- 480 Guieu, C., D'Ortenzio, F., Dulac, F., Taillandier, V., Doglioli, A., Petrenko, A., Barrillon, S., Mallet, M., Nabat, P.,
481 and Desboeufs, K.: Process Studies at the Air-Sea Interface After Atmospheric Deposition in the
482 Mediterranean Sea: Objectives and Strategy of the PEACETIME Oceanographic Campaign (May-June 2017),
483 *Biogeosciences Discuss.*, <https://doi.org/10.5194/bg-2020-44>, 2020.
- 484 Irish, V. E., Elizondo, P., Chen, J., Chou, C., Charette, J., Lizotte, M., Ladino, L. A., Wilson, T. W., Gosselin, M.,
485 Murray, B. J., Polishchuk, E., Abbatt, J. P. D., Miller, L. A., and Bertram, A. K.: Ice-Nucleating Particles in
486 Canadian Arctic Sea-Surface Microlayer and Bulk Seawater, *Atmos. Chem. Phys.*, 17, 10583-10595,
487 <https://doi.org/10.5194/acp-17-10583-2017>, 2017.
- 488 Knopf, D. A., Alpert, P. A., Wang, B., and Aller, J. Y.: Stimulation of Ice Nucleation by Marine Diatoms, *Nat.*
489 *Geosci.*, 4, 88-90, <https://doi.org/10.1038/ngeo1037>, 2011.
- 490 McCluskey, C. S., Hill, T. C. J., Malfatti, F., Sultana, C. M., Lee, C., Santander, M. V., Beall, C. M., Moore, K. A.,
491 Cornwell, G. C., Collins, D. B., Prather, K. A., Jayarathne, T., Stone, E. A., Azam, F., Kreidenweis, S. M., and
492 DeMott, P. J.: A Dynamic Link between Ice Nucleating Particles Released in Nascent Sea Spray Aerosol and
493 Oceanic Biological Activity during Two Mesocosm Experiments, *J. Atmos. Sci.*, 74, 151-166,
494 <https://doi.org/10.1175/JAS-D-16-0087.1>, 2017.
- 495 McCluskey, C. S., Hill, T. C. J., Sultana, C. M., Laksina, O., Trueblood, J. V., Santander, M. V., Beall, C. M.,
496 Michaud, J. M., Kreidenweis, S. M., Prather, K. A., Grassian, V. H., and DeMott, P. J.: A Mesocosm Double
497 Feature: Insights into the Chemical Makeup of Marine Ice Nucleating Particles, *J. Atmos. Sci.*, 75, 2405-
498 2423, <https://doi.org/10.1175/JAS-D-17-0155.1>, 2018a.
- 499 McCluskey, C. S., Ovadnevaite, J., Rinaldi, M., Atkinson, J., Belosi, F., Ceburnis, D., Marullo, S., Hill, T. C. J.,
500 Lohmann, U., Kanji, Z. A., O'Dowd, C., Kreidenweis, S. M., and DeMott, P. J.: Marine and Terrestrial Organic
501 Ice-Nucleating Particles in Pristine Marine to Continentally Influenced Northeast Atlantic Air Masses, *J.*
502 *Geophys Res. Atmos.*, 123, 6196-6212, <https://doi.org/10.1029/2017JD028033>, 2018b.



- 503 McCluskey, C. S., DeMott, P. J., Ma, P. L., and Burrows, S. M.: Numerical Representations of Marine
504 Ice-Nucleating Particles in Remote Marine Environments Evaluated Against Observations, *Geophys Res.*
505 *Let.*, 46, 7838-7847, <https://doi.org/10.1029/2018GL081861>, 2019.
- 506 McCoy, D. T., Hartmann, D. L., Zelinka, M. D., Ceppi, P., and Grosvenor, D. P.: Mixed-phase Cloud Physics and
507 Southern Ocean Cloud Feedback in Climate Models, *Journal of Geophysical Research: Atmospheres*, 120,
508 9539-95554, <https://doi.org/10.1175/JAS-D-17-0155.1>, 2015.
- 509 McCoy, D. T., Tan, I., Hartmann, D. L., Zelinka, M. D., and Storelvmo, T.: On the Relationship Among Cloud Cover,
510 Mixed-phase Partitioning and Planetary Albedo in GCMs, *Journal of Advances in Modeling Earth Systems*, 8,
511 650-668, <https://doi.org/10.1002/2015MS000589>, 2016.
- 512 Pujo-Pay, M., Conan, P., Oriol, L., Cornet-Barthaux, V. C., Falco, C., Ghiglione, J.-F., Goyet, C., Moutin, T., and
513 Prieur, L.: Integrated Survey of Elemental Stoichiometry (C, N, P) from the Western to Eastern
514 Mediterranean Sea, *Biogeosciences*, 8, 883-899, <https://doi.org/10.5194/bg-8-883-2011>, 2011.
- 515 Rogers, D. C., DeMott, P. J., Kreidenweis, S. M., and Chen, Y.: Measurements of Ice Nucleating Aerosols During
516 SUCCESS, *Geophys. Res. Lett.*, 25, 1383-1386, <https://doi.org/10.1029%2F97GL03478>, 1998.
- 517 Schnell, R. C., and Vali, G.: Biogenic ice Nuclei: Part I. Terrestrial and Marine Sources, *J. Atmos. Sci.*, 33, 1554-
518 1564, [https://doi.org/10.1175/1520-0469\(1976\)033%3C1554:BINPIT%3E2.0.CO;2](https://doi.org/10.1175/1520-0469(1976)033%3C1554:BINPIT%3E2.0.CO;2), 1976.
- 519 Schwier, A. N., Rose, C., Asmi, E., Ebling, A. M., Landing, W. M., Marro, S., Pedrotti, M.-L., Sallon, A., Iuculano, F.,
520 Agusti, S., Tsiola, A., Pitta, P., Louis, J., Guieu, C., Gazeau, F., and Sellegri, K.: Primary Marine Aerosol
521 Emissions from the Mediterranean Sea During Pre-Bloom and Oligotrophic Conditions: Correlations to
522 Seawater Chlorophyll-a From a Mesocosm Study, *Atmos. Chem. Phys.*, 15, 7961-7976,
523 <https://doi.org/10.5194/acp-15-7961-2015>, 2015.
- 524 Stopelli, E., Conen, F., Zimmermann, L., Alewell, C., and Morris, C. E.: Freezing Nucleation Apparatus puts New
525 Slant on Study of Biological Ice Nucleators in Precipitation, *Atmos. Meas. Tech.*, 7, 129-134,
526 <https://doi.org/10.5194/amt-7-129-2014>, 2014.
- 527 Thornton, D. C. O.: Dissolved Organic Matter (DOM) Release by Phytoplankton in the Contemporary and Future
528 Ocean, *European Journal of Phycology*, 49, 20-46, <https://doi.org/10.1080/09670262.2013.875596>, 2014.
- 529 Tovar-Sanchez, A., Arrieta, J. M., Duarte, C. M., and Sanudo-Wilhelmy, S. A.: Spatial Gradients in Trace Metal
530 Concentrations in the Surface Microlayer of the Mediterranean Sea, *Front. Mar. Sci.*, 1, 1-8,
531 <https://doi.org/10.3389/fmars.2014.00079>, 2019.
- 532 Vali, G.: Quantitative Evaluation of Experimental Results on the Heterogeneous Freezing Nucleation of
533 Supercooled Liquids, *J. Atmos. Sci.*, 28, 402-409, 1971.
- 534 Vergara-Temprado, J., Murray, B. J., Wilson, T. W., O'Sullivan, D., Browse, J., Pringle, K. J., O'Sullivan, D., Browse,
535 J. P., K. J., Ardon-Dryer, K., Bertram, A. K., Burrows, S. M., Ceburnis, D., DeMott, P. J., Mason, R. H., O'Dowd,
536 C. D., Rinaldi, M., and Carslaw, K. S.: Contribution of Feldspar and Marine Organic Aerosols to Global Ice
537 Nucleating Particle Concentrations, *ACP*, 17, 3637-3658, <https://doi.org/10.5194/acp-17-3637-2017>, 2017.
- 538 Verheggen, B., Cozic, J., Weingartner, E., Bower, K., Mertes, S., Connolly, P., Gallagher, M., Flynn, M.,
539 Choularton, T., and Baltensperger, U.: Aerosol Partitioning Between the Interstitial and the Condensed
540 Phase in Mixed-phase Clouds, *J. Geophys. Res.*, 112, <https://doi.org/10.1029/2007JD008714>, 2007.
- 541 Wilson, T. W., Ladino, L. A., Alpert, P. A., Breckels, M. N., Brooks, I. M., Browse, J., Burrows, S. M., Carslaw, K. S.,
542 Huffman, J. A., Judd, C., Kilhau, W. P., Mason, R. H., McFiggans, G., Miller, L. A., Nájera, J. J., Polishchuk, E.,
543 Rae, S., Schiller, C. L., Si, M., Vergara Temprado, J., Whale, T. F., Wong, J. P. S., Wurl, O., Yakobi-Hancock, J.
544 D., Abbatt, J. P. D., Aller, J. Y., Bertram, A. K., Knopf, D. A., and Murray, D. J.: A Marine Biogenic Source of
545 Atmospheric Ice-Nucleating Particles, *Nature*, 525, 234-238, <https://doi.org/10.1038/nature14986>, 2015.
- 546